Polymer Bulletin
https://doi.org/10.1007/s00289-024-05546-w

ORIGINAL PAPER

Rubber-based piezoresistive sensing: a new approach based on hydrodynamic flow of material deformation describing nonlinear signals in stretchable sensors

Evghenii Harea[1] · Sanjoy Datta[1] · Jaroslav Maloch[1] · Martin Stěnička[1] · Radek Stoček[1]

Received: 4 September 2024 / Revised: 15 October 2024 / Accepted: 17 October 2024

Abstract
The nonlinearity of piezoresistive response is critical in developing strain sensors, various self-monitoring applications and wearable electronics based on filled rubbers. This parameter could change dramatically when scaling up from small-size prototypes to full-scale production. The present work focuses on the nonlinear signals in stretchable rubber-based sensors, their origin and dependence on size of samples. Thus, a set of rectangular, piezoresistive samples differing in width was prepared from natural rubber reinforced with carbon black filler. Their electric resistance was tested under planar strain/recovery conditions at 25 and 50% strain amplitudes. It was found that piezoresistance and the related nonlinear phenomena significantly depended on the size of the samples. For the first time, hydrodynamic flow of deformed material was used to explain the nonlinearities of the piezoresistive signal. The trajectory, velocity, and magnitude of this flow were accounted for by a newly developed empirical equation describing the evolution of local resistivity under the strain/recovery process.

Keywords Nonlinear piezoresistance · Stretchable sensors · Filled rubber · Planar strain · Hydrodynamic pressure

Introduction

Traditionally, electrical properties of rubber compounds have been intensely investigated in the context of antistatic or insulating applications [1]. However, interest has gradually shifted to strain gauge sensors [2–4], sensors for supporting mobility

✉ Evghenii Harea
harea@utb.cz

[1] Centre of Polymer Systems, University Institute, Tomas Bata University in Zlín, tř. Tomáše Bati 5678, 76001 Zlín, Czech Republic

Published online: 05 November 2024

[5], self-monitoring the behavior of filler network [6], fatigue life prediction [7, 8], soft robotics actuators [9, 10] and the like, commonly based on piezoresistive effect in rubbers filled with various conductive fillers. However, the present study goes beyond these applications, exploring the possibilities of scaling up the developed prototypes and the corresponding nonlinearities in the piezoresistive signal.

Over the years, different non-conductive rubber matrices loaded with various conductive fillers at different concentrations were used as a structural material for prototyping various electromechanical devices. Simultaneously, some theories explaining their piezoresistive behaviors, including nonlinear phenomena [7, 11–22], were propounded. The highly nonlinear piezoresistivity of CB-filled rubber got seriously known after Yamaguchi et al. published their research [13] in 2003. The authors observed that electrical resistivity increased when a filled elastomer specimen was stretched to small extensions and, contrary to that, decreased at higher tensile extensions, which was ascribed to the initial breakdown of the carbon black network structure and further alignment of the shaped CB aggregates under strain at that time being only an observed phenomenon. However, the phenomenon asked for a more detailed explanation, which was later substantiated through the work [7] and called precursor of shoulder peak phenomenon (PSPP). Following the strain, the samples exhibited another nonlinear phenomenon—a jump in electrical resistance in the recovery phase, coined later as shoulder peak phenomenon (SPP). Their origin has been granted to filler dynamics without too much detailed explanation. Often, the SPP is described in the following string of words: "The shoulder peak phenomenon is mainly caused by the competition between the destruction and reformation of the conductive network during the deformation and the time-dependent properties (viscoelasticity) of the polymer matrix" [15]. Thus, a deep understanding of filler dynamics is further necessary for an adequate quantification of nonlinear piezoresistive signal.

The filler dynamics, which refer to the movement and rearrangement of the conductive fillers within the rubber matrix, are highly influenced by polymer-filler interphase interaction, which governs the structure and properties of composites [23–26]. Here, the dominant microscopic mechanisms are the hydrodynamic effect and stiff interphases bonding the elastomer to the fillers [27]. All the models regarding the deformation of such composites contain the assumption of geometrical arrangements of aggregates or filler network structures resulting from percolation or kinetical flocculation. These concepts are primarily independent of filler types [24] and satisfactorily predict the Payne effect [28].

Directly monitoring filler dynamics during the deformation of the sample is challenging [26]. In the present study, a non-trivial approach to estimating the filler dynamics using digital image correlation (DIC) of the surface material flow of a deformed planar specimen was applied to overcome this difficulty. The straining of the planar specimen always divides the sample into three regions: namely, a region of pure shear (PS) and two symmetric regions of lateral contraction (LC) (Fig. 1). From a mechanical perspective, the specimen is strained primarily in the direction of the tensile deformation within the width of the PS region. A randomly selected surface of $w_0 \times l_0$ deforms into $w_0 \times l$, indicating that the distances between the individual particles, aggregates, and agglomerates composing the conductive fillers

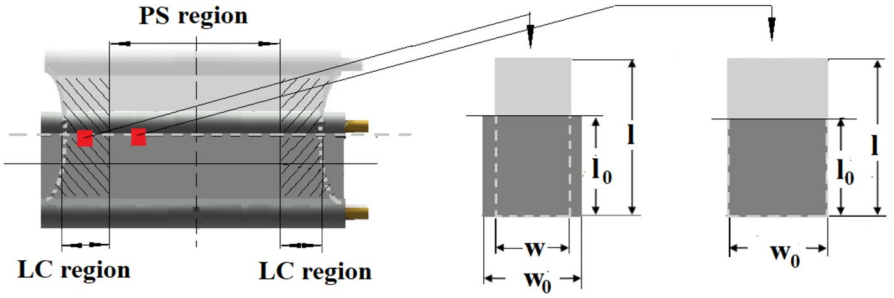

Fig. 1 Representation of the planar sample indicating PS and LC regions possessing different hydrodynamic behaviors

increase in the direction of the applied strain without any significant perpendicular movement. In the edge regions, the deformation involves tension in the stretching direction and contraction in the perpendicular direction, transforming any surface of $w_0 \times l_0$ into $w \times l$. Similarly, the distances between the filler particles increase in the direction of the principal strain, but they converge in the perpendicular direction. This unique deformation, where the size of the regions depends on scaling up preferences and can be unambiguously determined by using DIC, has led us to devise a novel tool. This tool, which enables us to analyze the CB-reinforced rubber's electrical properties through differential filler dynamics, provides a precise and reliable approach in our field.

The present work reports findings on piezoresistivity of natural rubber (NR) filled with 60 phr of CB, which is unusually high concentration for electro-sensitive but usual for many industrial rubber applications. Samples, designated as NR9, NR7, NR5, and NR3, were filled with CB type N330. They had a fixed length L_0 of 10 mm and fixed thickness, of 2 mm, but varying widths W_0 of 90, 70, 50, and 30 mm. The piezoresistance as a function of sample size was investigated under a strain/recovery experiment at moderate strain amplitudes of 25 and 50%, which are well below the strain level at which crystallization occurs in NR.

Experimental

Materials

Rubber compounding was done in a two-stage mixing process. In the first stage, masterbatches were prepared by mixing the natural rubber (NR) SMR20 CV/BP1 (Lee Rubber Co. (Pte) Ltd. Malaysia) with the reinforcing and electrically conducting high abrasion furnace (HAF) (N330) carbon black (CB) filler, supplied by Cabot Corporation, Boston, MA, USA.

In continuation, the second mixing stage was achieved by the addition of curing ingredients as follows: sulfur, zinc oxide (ZnO), stearic acid and 6PPD (N-(1,3-dimethylbutyl)-N′-phenyl-p-phenylenediamine) were supplied by Sigma-Aldrich,

Germany, while TBBS (N-tert-butyl-benzothiazolesulfenamide) was produced by Xianyang Sanjing Technology Co, China. The final prepared batch was milled and sheeted in a two-roll mill and stored for 24 h at an ambient temperature of 23 °C before the rheological investigation and further curing. The complete formulation of the rubber compound produced and used for this study is listed in Table 1.

The optimum cure time (OCT) of 5.37 min at 160 °C was determined using a moving die rheometer (MDR 3000, MonTech, Germany) according to ISO 3417. Based on the OCT, the compound was molded in an electrically heated hydraulic press (LabEcon, The Netherland) at 160 °C and 200 kN into samples of a specific geometry, defined generally with dimensions of $90 \times 10 \times 2$ mm^3 with cylindrical shoulders of 6 mm diameter at both the ends of the long side. A brass tube (outer diameter 2 mm and inner diameter 1.4 mm) was vulcanized into each cylinder to implement future electrical contacts, as shown in Fig. 1. Samples of the width, $W_0 = 90$, 70, 50 and 30 mm and length, $L_0 = 10$ mm, were cut from the initially prepared dimensioned sample. Therefore, samples with varied aspect ratios, $W_0/L_0 = 9$, 7, 5 and 3, were at disposal for future analysis. Three replicates from each aspect ratio were prepared and tested.

Experimental setup

The customized experimental setup for direct current (DC) resistance measurements used in this study has been described in detail in a previous work [14]. All data were recorded with a digital multichannel oscilloscope RIGOL MS05104 (RIGOL TECHNOLOGIES, Co Ltd, China). In order to achieve an accurate time synchronization of the sampled data, each of the physical quantities (force, displacement, current and voltage) was recorded from one of the four channels of the oscilloscope.

The samples' mechanical deformation was efficiently achieved using servo-hydraulic tensile testing equipment, Instron 8871 (Instron, UK), equipped with modified non-conductive clamps as in [14]. These clamps were used to fix the lateral cylindrical shoulders of the tested samples, effectively reducing the additional stress commonly encountered with simple fixing. The conductive wires were mechanically crimped into the brass tubes, a method that avoided metal-rubber interface overheating, a potential disadvantage of soldering. This efficient process ensured the validity of our experimental conditions.

A triangular loading protocol consisting of 25% and 50% strain and strain recovery phases was used to monitor the electrical response of the specimens at a specified strain rate.

Table 1 Rubber formulation

1st stage		2nd stage				
NR*	Carbon black*	TBBS*	Sulfur*	ZnO*	Stearic Acid*	6PPD*
100.00	60.00	1.00	2.00	2.00	1.00	1.00

*phr—parts per hundred of rubber by mass

The local hydrodynamic flow of the samples was monitored by a digital image correlation (DIC) system. For this purpose, a stochastic pattern made by an anti-reflex spray, MR2000 Anti-Reflex L (MR Chemie GmbH, Unna, Germany), was applied on the surface of all the tested samples. Complete strains of the samples were recorded over the testing protocols via a charge-couple device (CCD) monochrome camera Baeumer PXU 60 M Q (Bauemer, Frauenfeld, Switzerland) with a sampling frequency of 15 Hz. The DIC process was controlled using the software GOM Snap 2D (GOM, Braunschweig, Germany) and trajectories of points with 2-mm separation, situated on the axis perpendicular to the stretching direction, were meticulously tracked. This monitoring process ensured the comprehensiveness of the obtained data.

Moreover, a JEOL 1200 EX (LEOL, Japan) microscope, operating at a 120 kV acceleration voltage, was employed to capture transmission electron microscope (TEM) images of the carbon black-rubber interphase. CB dispersed in toluene was drop-casted on carbon-coated copper grids and air-dried at room temperature. For interphase shell investigation, 1 g of a thoroughly mixed uncured rubber composite was dissolved in 20 ml of toluene for one week. The obtained solution was then homogenized in an ultrasound bath for 30 min. 0.02 ml of the attained solution was further dissolved into 1 ml of toluene, drop-casted on the carbon-coated copper grids and air-dried at room temperature for 72 h.

Results and discussion

Figure 2a and b shows the representative force versus time curves for all the phases of the testing protocols of the investigated samples. Since the initial length of samples was kept constant, the force required to deform the specimens to the set deformation was a function of the width, with a known and expected trend of an increase in force with an increase in cross section. For example, specimen NR3 exhibited forces of approximately 20 N and 30 N at 25% and 50% strain, respectively, which were much less compared to those of the specimen NR9 which exhibited approximately 55 N and 84 N for the respective strains.

For all the tested specimens, a transition to a negative force was observed just before the fixing clamps returned to their initial positions. This opposing force generally defeats the temporary residual strain of a crosslinked rubber matrix. It lasts until the rubber molecules completely relax and get accommodated to the new state of maximum entropy attained at equilibrium [7].

The representative piezoresistive responses of the samples, as shown in Fig. 2c and d, clearly demonstrate the alternation of resistance trend during the loading sequence, followed by an increase in resistance during the strain recovery stage. These nonlinear phenomena, referred to as PSPP and SPP in this study, are evident and strongly influenced by the sample size and corresponding filler dynamics.

PSPP [7] can be understood as a situation where a part of the electric resistance is seemingly withdrawn and stored until the strain is released. At this point, the electric resistance, instead of continuously decreasing, experiences a sudden increase, known as the SPP. Thus, the recovery phase was characterized by

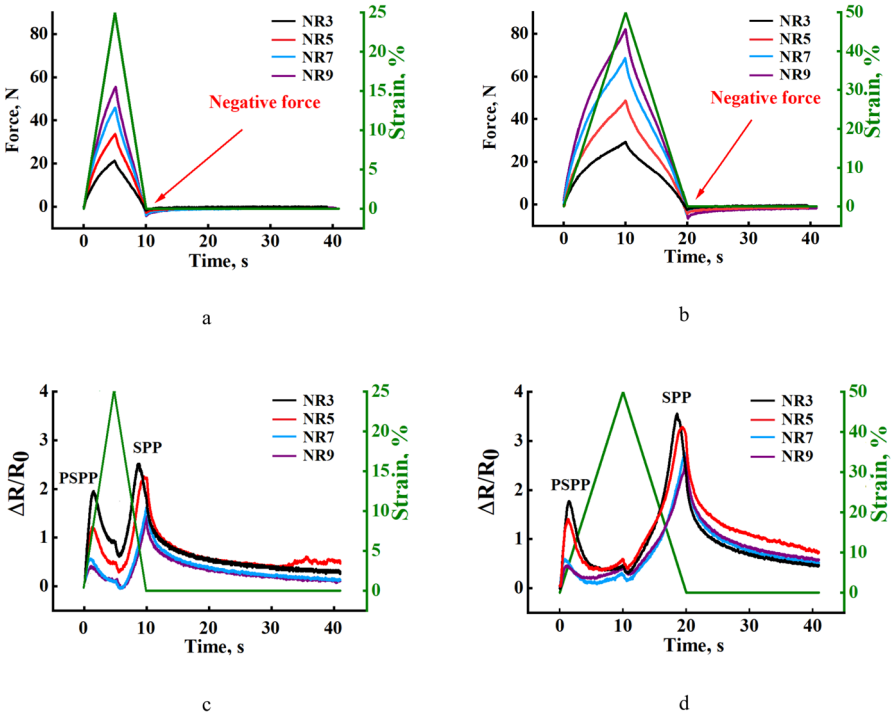

Fig. 2 Applied tensile force versus time and strain for different size of the samples strained up to **a** 25% and **b** up to 50%. Piezoresistive response of tested samples up to **c** 25% strain amplitude and up to **d** 50% strain amplitude

a remarkable shoulder peak phenomenon (SPP), as shown in Fig. 2c and d. PSPP and SPP phenomena were consistently observed in the applied test protocols and for all aspect ratios of tested samples. Notably, the specimens with higher aspect ratios exhibited a lower resistance amplitude of piezoresistive nonlinearities. In each case, the electric resistance at the maximum strain was much smaller than that of the peak resistance during PSPP or SPP.

As the introduction mentions, different aspect ratios in the specimens resulted in different ratios between the LC and PS regions. The widths of the PS and LC regions at the maximum strains used in the test protocols were calculated according to references [29, 30] and presented in Table 2. A tolerance of 1% was chosen for all calculations to ensure minimum deviation.

An essential conclusion can be drawn: The ratio between LC and PS regions strongly affects the magnitude of the nonlinear piezoresistive signals. Specifically, a higher ratio generates a higher amplitude of the nonlinear signal.

The obtained results revealed a much higher degree of nonlinearity of piezoresistance at the recovering stage compared to that in the stretching process. Another significant conclusion emerged: The filler moved along distinct trajectories during the stretching and relaxation stages. DIC technology, a reliable and

Table 2 Width of PS region and LC regions and their ratio at maximum applied strains

Sample	NR3	NR5	NR7	NR9
PS region (mm)	3.7	7.1	11.9	25.1
LC at 25% strain, (mm)	12.6	20.3	28.3	31.6
LC at 50% strain, (mm)	12.0	19.2	27.6	30.9
2*LC/PS, at 25%	6.8	5.7	4.7	2.5
2*LC/PS, at 50%	6.5	5.5	4.6	2.4

accurate method, was employed to confirm this. The remarkable results showed two different trajectories for the stretching and recovering stages. Moreover, and very importantly, the differences gradually decreased from the edge of the LC region toward the PS region, as shown in Fig. 3, where sample NR 5 was taken as the representative one.

The trajectories of surface points aptly traced by using DIC, conclusively represented an in-plane projection of the filler motion. At the edge of the sample, a significant lateral displacement was noted at the onset of deformation in the LC region (see the trajectories of filler within strips number 1, 2 and 3 in Fig. 3b). This lateral deformation gradually decreased from the edge of the PS toward the center of the sample and became almost zero at the PS region. This fact led to a local increase in the volume fraction of the conductive CB filler. As per the percolation threshold theory, this increase in the filler volume fraction in the rubber matrix could transform the low conductivity, implemented through the tunneling of electrons between conductive particles, to a higher conductivity, depending on the junction width.

This dynamic behavior made the electric charges reorient and flow more accessible through the recently modified, more conductive paths, producing a PSPP. Later, the effective electric resistance suddenly increased with the initiation of the sample's recovery, generating the SPP. It was hypothesized that in general SPP most probably happens due to the tendency for a fast destruction of "superconductive" peripheral paths in the LC region. It was then the confrontation between the evolution of resistances in LC and PS regions which formed the final shape of PSPP and SPP. This was the key finding in the present study.

The assumption of local fluctuation of filler volume fraction and the proof of the duality of filler dynamics during the stretching and recovery stages provides valuable insights into the mechanism of the occurrence of nonlinear piezoresistive effects and their evident asymmetry. However, the challenge to understand the immense amplitude of the nonlinear signals, which clearly exceed the resistance at maximum strain, remains unanswered. This underscored the need for a more profound insight into the material's structure.

The filler reinforcement theory suggests that a modified rubber shell should be formed around the CB particles or aggregates (the so-called interphase shell) [23, 27, 31]. Thus, this shell can be formed by the adsorption of the elastomer chains onto CB surfaces, by the free radical chemistry that can occur between polymer chains and CB aggregates, or through some chemical bonds between polymer and filler without chain adsorption [31]. In any case, these shells should have their input

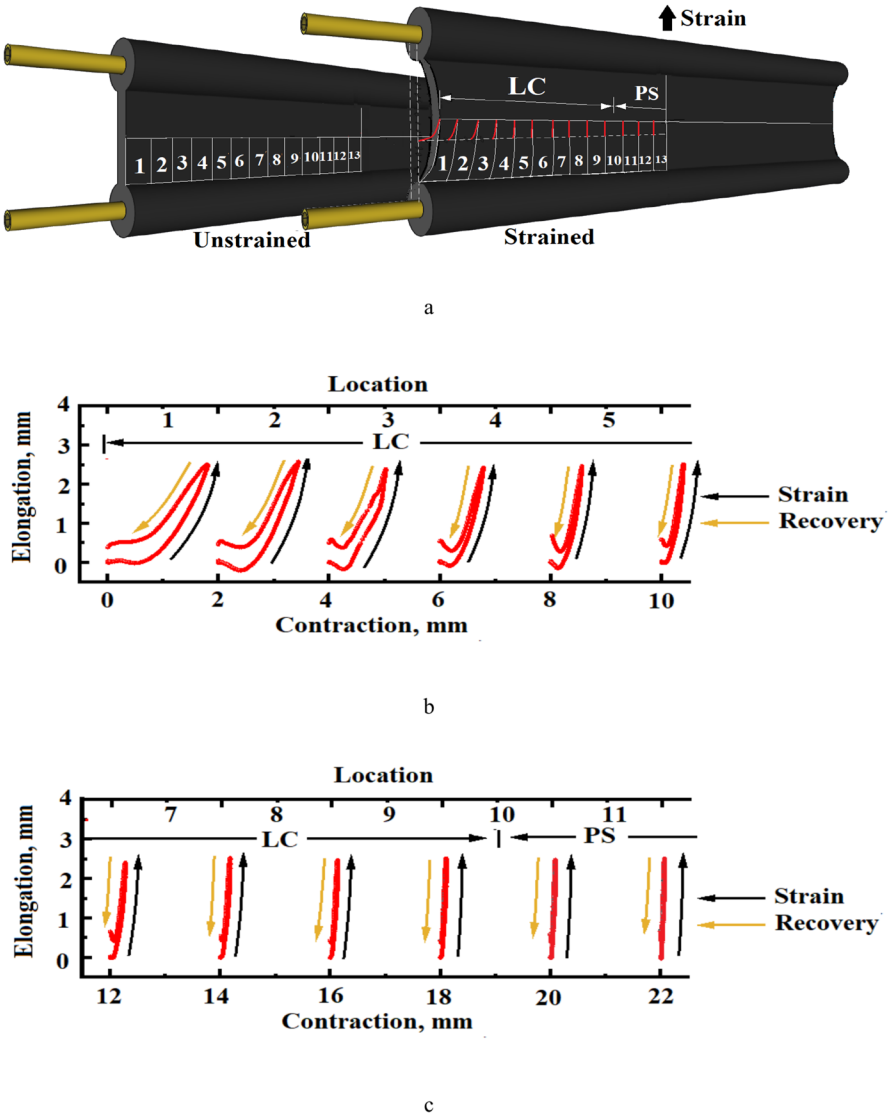

Fig. 3 **a** Schematic of unstrained and up to 50% strained NR5 specimen with corresponding trajectories of selected points traced by DIC. **b** and **c** are magnified trajectories of selected points during the deformation and recovery processes

into junction width formation and, consecutively, should influence the effective electric resistance, leaving much less room for the variation of junction width during the deformation.

The present study shows the TEM images of the CB agglomerates without and with interphase shells; the latter exhibited almost twice the size of the CB filler (see Fig. 4). Observed shells, taken as a difference between the initial CB particle

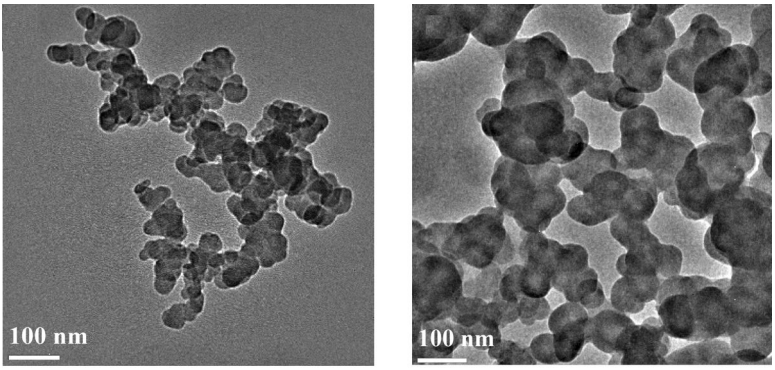

Fig. 4 TEM images of CB N330 agglomerates: **a** before mixing, **b** extracted by dissolving the uncured composite in toluene

sizes (around 30 nm for CB N330) and those extracted after compounding, had a 10–15 nm thickness. These shells, intriguingly, could not be formed from a mere modification of rubber. The reasons were twofold: firstly, the solvent proved ineffective in dissolving these shells, and secondly, for such junction dimensions between CB aggregates, the tunneling effect, and resulting effective conductivity, must be negligibly small [32].

Hence, the formed shells were not a part of non-conductive barriers and must have possessed a reasonable electric conductivity. Simultaneously, their mechanical and chemical behaviors diverged significantly from the rest of the rubber matrix. This led to the conclusion that the shells were most likely a part of a former CB particle, swollen by deep adsorption and penetration of rubber molecules into the CB surface. However, it is important to note that another intriguing possibility, such as the synthesis of a new conductive polymer on the CB surface, cannot be excluded, highlighting the need for further investigation.

Considering the hypothesis about the conductivity of the interphase shells, their remarkable resistance to solvents, and their resistance to mechanical breakage, it is challenging to fathom that an aggregate of CB protected by such a shell can be broken at small deformations, thus generating the PSPP drop in resistance. This finding in the present work could potentially revolutionize the understanding of the behavior of carbon black particles in a rubber matrix, opening up new avenues for research and application in the field of composite materials.

In such circumstances, the breakage of filler aggregates, as a primary mechanism of nonlinearities in piezoresistance, propounded in the past, may be incorrect. However, torsion and distance variation between aggregates in deformed samples are undebatable contributors to nonlinear signals, but they cannot be responsible for the extreme amplitude of signals as long as the intrinsic behavior of CB is not considered. Thus, the variation of intrinsic resistivity of CB aggregates covered by interphase shell is a concept that could complement the percolation theory and can play

a significant role in accounting for the sudden variation in the electrical resistance during the deformation of the sample.

The well-known formula for percolation threshold in terms of resistivity can be written as:

$$\rho = \rho_0 \left(v - v_c\right)^{-\tau} \tag{1}$$

where ρ is the electrical resistivity, ρ_0 is the scaling factor, ν is the volume fraction of the conductive filer, ν_c is the critical volume fraction of the filler for the electrical percolation threshold, and $\tau = 1.6$ [33] is the conductivity exponent. During the deformation of the sample, the hydrodynamic pressure may dramatically change the intrinsic resistivity of the CB aggregate [34–36], affecting the effective resistance of the whole sample. Thus, the scaling factor ρ_0 becomes pressure-dependent and could be substituted by the intrinsic resistivity ρ_i of CB [35]:

$$\rho_i = \frac{K}{P^n} + J \tag{2}$$

where P is the applied pressure, K and J are the coefficients, and n has values between 1 and 2 in dependence on the elasticity or the plasticity of the reinforcing and conducting particles. Usually, the structure of carbon black is considered to be a heterogeneous mixture of domains that range from a single graphite layer (graphene) to graphite crystals [37]. Consequently, the intrinsic resistivity is also dependent on pressure orientation. Although pressure does not follow the vector laws, it can be said that the direction and magnitude of pressure depend upon the orientation of the surface of graphite crystallites [38]. In the case of a sample under deformation, it is now assumed that the pressure varies due to the internal hydrodynamic effect and the terms from Eqs. (1) and (2) can then be considered to be strain (ε) dependent. Thus,

$$\rho(\varepsilon) = \rho_i(\varepsilon)\left[v(\varepsilon) - v_c\right]^{-\tau} = \left(\frac{K}{P(\varepsilon)^n} + J\right)\left[v(\varepsilon) - v_c\right]^{-\tau} \tag{3}$$

The hydrodynamic pressure *P(ε)* can be expressed through instantaneous speed of hydrodynamic flow *U(ε):*

$$P(\varepsilon) = \rho^* \frac{U(\varepsilon)^2}{2} \tag{4}$$

where ρ^* is the density of rubber matrix. The formula for the calculation of the local resistivity, which now consider both, the filler dynamics and the intrinsic quantum effects within the filler, can be written as:

$$\rho(\varepsilon) = \left(\frac{2^n K}{\rho^{*n} U(\varepsilon)^{2n}} + J\right) \cdot \left[v(\varepsilon) - v_c\right]^{-\tau} \tag{5}$$

Resulting from Eq. (5), the resistivity in a certain place of the sample under deformation can be seen to be dependent on the local speed of hydrodynamic

flow and the local volume fraction of the CB filler in a rubber composite. Both the local speed of hydrodynamic flow and the local filler volume fraction in the samples under deformation are dependent on the sample size and could be found from DIC measurements.

The complicated calculation to find the effective resistance of the entire sample under deformation was sidestepped in this paper, being a matter of a separate research. Instead, the analysis of dynamic filler volume fraction and the corresponding hydrodynamic pressure in the discrete regions (as denoted in Fig. 3a) from the edge toward the middle of the sample was performed. Therefore, one-fourth of the sample was imaginatively divided into 2-mm-wide strips covering the LC region and the half-width of the PS region.

For simplicity, all the material within one such a strip was considered to move parallel to the material on the surface, and the thickness of the sample under deformation was considered to be a constant at 2 mm. Hence, the measured displacement of the upper left corner of each strip allowed to assess the instantaneous changes in its volume V_s under strain. The strain-dependent filler volume fraction presented in Fig. 5 is calculated as:

$$v(\varepsilon) = \frac{V_f}{V_s(\varepsilon)} \tag{6}$$

where $V_s(\varepsilon)$ is the volume of selected strip at a certain strain of the tested sample, and V_f is the volume of the CB filler occupying the examined region, considered to be a constant during the whole deformation process.

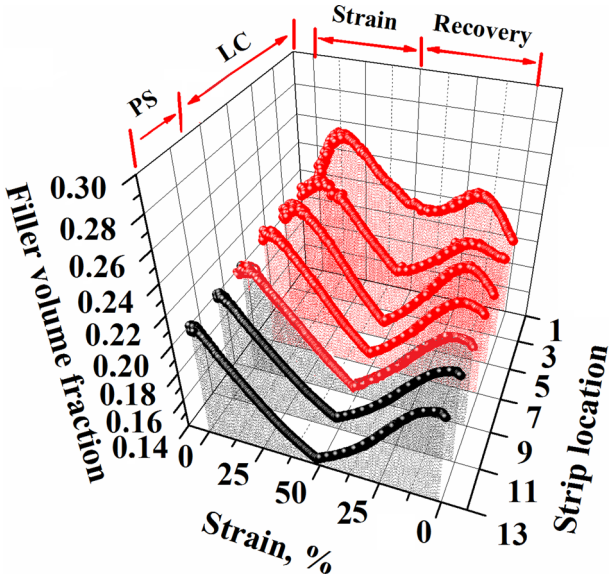

Fig. 5 Strain-dependent variation of filler volume fraction in selected strips

It should be noted that at the edge of the sample, a non-trivial behavior, such as an observable increase in the local filler volume fraction, was attested at the beginning of the sample strain and close to the end of the recovery process. However, in the end, this increase was comparatively less than that at the beginning.

Consequently, a hydrodynamic pressure gradient directed from the edge of the sample to the PS region was predictable. To determine the hydrodynamic pressure in the strips, the speed of displacement of each corresponding upper left corner relative to their initial position (Fig. 3a) was considered. Expectedly, the maximum hydrodynamic pressure was observed in the LC domain, gradually decreasing from the edge of the sample toward the PS domain (Fig. 6).

Strain-dependent hydrostatic pressure and filler volume fraction show an impressive dependence on the location of the examined strips, predicting an essential difference in local resistivity. In order to check this, a simplified approach was adopted, where the thickness of the sample was assumed to be a constant at 2 mm, and the constants from Eq. (5) were assumed to have the following values: $K=1$, $J=0$, while $n=1$. In such a context, Eq. (5) is reduced to the following:

$$\rho(\varepsilon) = \frac{1}{P_h(\varepsilon)} \cdot [v(\varepsilon) - v_c]^{-\tau} \tag{7}$$

where $P_h(\varepsilon)$ is the strain-dependent hydrodynamic pressure inside of the considered strip, Further, in the equation, $v_c=0.1$ [39] is critical filler volume fraction for percolation threshold, $v(\varepsilon)$ is the strain-dependent filler volume fraction for certain strip, and the conductivity exponent $\tau=1.6$ as established in [33]. The results are graphically presented in Fig. 7 and represent the trend observed in experimental

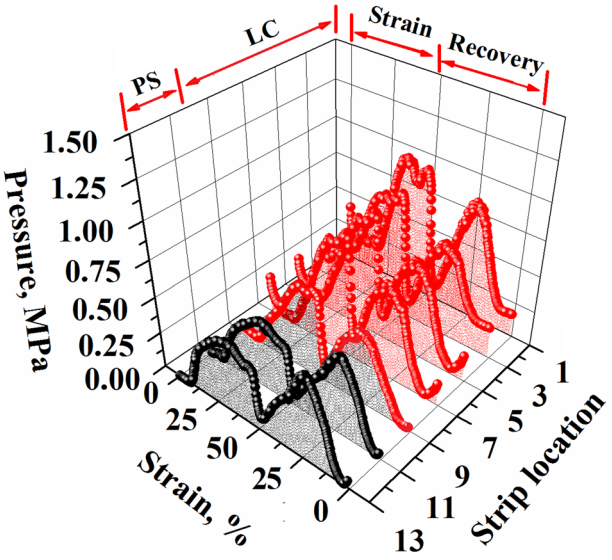

Fig. 6 Hydrodynamic pressure in the selected regions of the sample under strain history

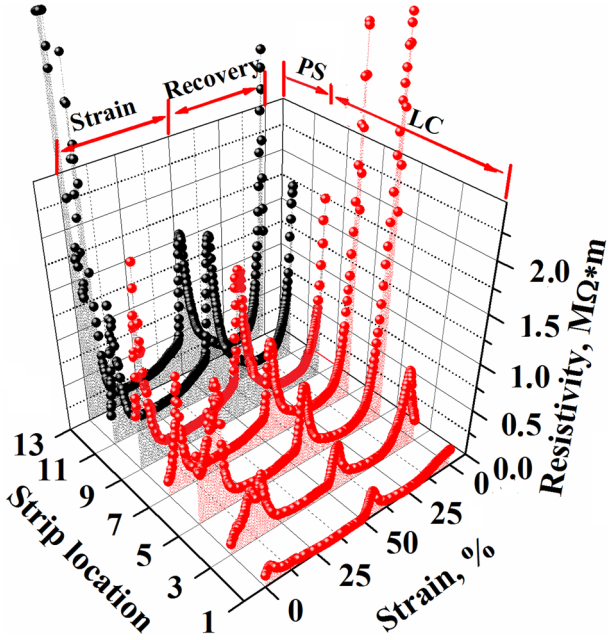

Fig. 7 Calculated local resistivity for selected regions

measurements. For all the analyzed strips, the resistivity increased at the beginning of deformation, followed by a deep decrease in resistivity, reflected by the generated PSPP effect.

The second explosion of resistivity was attested right after the start of strain recovery in the sample, expressed through SPP on the effective piezoresistance curve. Finally, a third increase in resistivity was observed during the residual strain overcoming when the tensile machine tried to return the fixing clamps to their initial positions. The last two resistivity jumps are superimposed on the effective piezoresistance curve and exhibit just one large shoulder peak phenomenon.

Interestingly, the PS region strips showed a much more significant increase in resistivity, which contradicted the results obtained for the PSPP effect, which is thought to have developed predominantly in the LC region. The explanation could be that due to an immense increase in resistivity in the PS region, the electric charges massively avoided this region and flowed mainly through the LC region, following the rules imposed by the hydrodynamic processes.

Thus, changing the sample size may change the amplitude of the piezoresistive signal and, even more unfortunately, may lead to the appearance of signal inhomogeneities such as the PSPP and SPP. Of course, with their rational explanation, these detectable signal inhomogeneities may be advantageously used in some future applications.

Conclusions

This study investigated the nonlinear phenomena of piezoresistive rectangular samples based on natural rubber filled with 60 phr of carbon black filler. The different sizes of the samples generated various amplitudes of the nonlinear piezoresistive signal due to the different ratios of PS and LC regions with specific strain-dependent hydrodynamic behavior.

The conducting paths inside the deformed specimen cannot be considered homogeneous within the whole matrix but have different instantaneous conductivity depending on their location, strain rate, strain amplitude, and sample size. The local variation of conductivity depends on two main size-dependent processes: filler dynamics in the rubber matrix and the change in intrinsic resistivity of the CB aggregates according to the surrounding hydrodynamic pressure.

The study calculated the instantaneous local filler volume fraction and hydrodynamic pressure based on DIC data. The calculated local strain-dependent resistivity had a sudden increase at the beginning of the sample strain and at the beginning of the recovery process, corresponding to the observed PSPP and SPP on the curve of piezoresistance.

Finally, it may be concluded that nonlinear piezoresistive phenomena are always present in rubber-based sensors. But these phenomena could be efficiently diminished by choosing a wright size of sample and filler concentration for certain range of deformation speeds. This is an undebatable fact that emerged from the study.

Acknowledgements This work was supported by the Ministry of Education, Youth and Sports of the Czech Republic – DKRVO (RP/CPS/2022/006).

Author contributions E.H. involved in conceptualization, methodology, investigation, validation, formal analysis, data curation, writing—original draft, and writing—review and editing. S.D. involved in writing—review and editing. J.M. involved in data curation. M.S. involved in data curation. R.S. involved in writing—review and editing and funding acquisition.

Funding Open access publishing supported by the National Technical Library in Prague.

Data availability No datasets were generated or analyzed during the current study.

Declarations

Conflict of interest The authors declare no competing interests.

References

1. Havranek A, Bakule RA (1967) Comparison of the viscoelastic and dielectric properties of natural rubber—sulfur systems. J Polym Sci Polym Symp 16:351–359. https://doi.org/10.1002/polc.5070160131
2. Zhao H, Bai J (2015) Highly sensitive piezo-resistive graphite nanoplatelet-carbon nanotube hybrids/polydimethylsilicone composites with improved conductive network construction. ACS Appl Mater Interfaces 7:9652–9659. https://doi.org/10.1021/acsami.5b01413
3. Bhagavatheswaran ES, Vaikuntam SR, Stöckelhuber KW, Wießner S, Heinrich G, Das A (2018) A High-performance elastomeric strain sensor based on nanostructured carbon fillers for potential tire applications. Mater Today Commun 14:240–248. https://doi.org/10.1016/j.mtcomm.2018.01.013
4. Harea E, Datta S, Stěnička M, Stoček R (2020) Undesirable aspects of fatigue on stretchable elastomer sensors. In: Petkov P, Achour M, Popov C (eds) In: Nanoscience and nanotechnology in security and protection against CBRN threats, vol 1. Springer, Dordrecht, pp 95–105
5. Yi J (2008) A Piezo-sensor-based, "smart tire" system for mobile robots and vehicles. IEEE/ASME Trans Mechatron 13:95–103. https://doi.org/10.1109/TMECH.2007.915064
6. Wießner S, Bhagavatheswaran ES, Stöckelhuber KW, Heinrich G, Das A (2020) Piezoresistivity—a powerful tool to monitor the behaviour of filler networks in rubber. AIP Conf Proc doi 10(1063/5):0028322
7. Harea E, Datta S, Maloch J, Stoček R (2023) Novel perspectives on self-monitoring internal rubber failure using piezoresistivity. Int J Fatigue 175:107825. https://doi.org/10.1016/j.ijfatigue.2023.107825
8. Harea E, Datta S, Stěnička M, Stoček R (2019) Electrical conductivity degradation of fatigued carbon black reinforced natural rubber composites: effects of carbon nanotubes and strain amplitudes. Express Polym Lett 13:1116–1124. https://doi.org/10.3144/expresspolymlett.2019.96
9. Banerjee S, Arief I, Rebecca Berthold R, Wiese M, Bartholdt M, Ganguli D, Mitra S, Mandal S, Wallaschek J, Raatz A, Heinrich G, Das A (2021) Super-elastic ultrasoft natural rubber-based piezoresistive sensors for active sensing interface embedded on soft robotic actuator. Appl Mater Today 25:101219. https://doi.org/10.1016/j.apmt.2021.101219
10. Banerjee SS, Mandal S, Arief I, Layek RK, Ghosh AK, Yang K, Kumar J, Formanek P, Fery A, Heinrich G, Das A (2021) Designing supertough and ultrastretchable liquid metal-embedded natural rubber composites for soft-matter engineering. ACS Appl Mater Interfaces 13:15610–15620. https://doi.org/10.1021/acsami.1c00374
11. Sichel EK (1982) Carbon black-polymer composites. The physics of electrically conducting composites. Dekker, New York
12. Tang H, Chen X, Tang A, Luo Y (1996) Studies on the electrical conductivity of CB-filled polymers. J Appl Polym Sci 59:383–387. https://doi.org/10.1002/(SICI)1097-4628(19960118)59:3%3c383::AID-APP1%3e3.0.CO;2-L
13. Yamaguchi K, Busfield JJC, Thomas AG (2003) Electrical and mechanical behavior of filled elastomers. I. The effect of strain. J Polym Sci, Part B: Polym Phys 41:2079–2089. https://doi.org/10.1002/polb.10571
14. Harea E, Datta S, Stěnička M, Maloch J, Stoček R (2021) The influence of local strain distribution on the effective electrical resistance of carbon black filled natural rubber. Polymers 13:2411. https://doi.org/10.3390/polym13152411
15. Yang H, Yuan L, Yao XF, Zheng Z, Fang DN (2020) Monotonic strain sensing behavior of self-assembled carbon nanotubes/graphene silicone rubber composites under cyclic loading. Compos Sci Technol 200:108474. https://doi.org/10.1016/j.compscitech.2020.108474
16. Chen J, Li H, Yu Q, Hu Y, Cui X, Zhu Y, Jiang W (2018) Strain sensing behaviors of stretchable conductive polymer composites loaded with different dimensional conductive fillers. Compos Sci Technol 168:388–396. https://doi.org/10.1016/j.compscitech.2018.10.025
17. Zhang S, Sun K, Liu H, Chen X, Zheng Y, Shi X, Zhang D, Mi L, Liu C, Shen C (2020) Enhanced piezoresistive performance of conductive WPU/CNT composite foam through incorporating brittle cellulose nanocrystal. Chem Eng J 387:124045. https://doi.org/10.1016/j.cej.2020.124045
18. Tang J, Wu Y, Ma S, Yan T, Pan Z (2023) Strain-sensing composite nanofiber filament and regulation mechanism of shoulder peaks based on carbon nanomaterial dispersion. ACS Appl Mater Interfaces 15:7392–7404. https://doi.org/10.1021/acsami.2c20390

19. Lin Y, Dong X, Liu S, Chen S, Wei Y, Liu L (2016) Graphene-elastomer composites with segregated nanostructured network for liquid and strain sensing application. ACS Appl Mater Interfaces 8:24143–24151. https://doi.org/10.1021/acsami.6b08587
20. Yang H, Feng X, Zhong Y, Ling Z, Gong H, Yuan L, Nan Y, Ying Y, Liu H (2018) Highly sensitive and stretchable graphene-silicone rubber composites for strain sensing. Compos Sci Technol 167:371–378. https://doi.org/10.1016/j.compscitech.2018.08.022
21. Mersch J, Winger H, Nocke A, Cherif C, Gerlach G (2020) Experimental investigation and modeling of the dynamic resistance response of carbon particle-filled polymers. Macromol Mater Eng 305:2000361. https://doi.org/10.1002/mame.202000361
22. Cui X, Jiang Y, Xu Z, Xi M, Jiang Y, Song P, Zhao Y, Wang H (2021) Stretchable strain sensors with dentate groove structure for enhanced sensing recoverability. Compos B Eng 211:108641. https://doi.org/10.1016/j.compositesb.2021.108641
23. Wilke LA, Robertson CG, Karsten DA, Hardman NJ (2023) Detailed understanding of the carbon black–polymer interface in filled rubber composites. Carbon 201:520–528. https://doi.org/10.1016/j.carbon.2022.09.032
24. Heinrich G, Klüppel M (2002) Recent advances in the theory of filler networking in elastomers. In: Abe A, Albertsson AC, Cantow HJ (eds) In: Filled elastomers drug delivery systems advances in polymer science, vol 160. Springer, Berlin, pp 1–44
25. Fleck F, Froltsov V, Klüppel M (2014) Polymer-filler interphase dynamics and reinforcement of elastomer nanocomposites. Soft Matter 12:S121–S134. https://doi.org/10.1080/1539445X.2014.957836
26. Presto D, Narayanan S, Moctezuma S, Sutton M, Foster MD (2023) Microscopic origins of the nonlinear behavior of particle-filled rubber probed with dynamic strain XPCS. ACS Appl Mater Interfaces 15:22714–22729. https://doi.org/10.1021/acsami.3c01955
27. Goudarzi T, Spring DW, Paulino GH, Lopez-Pamies O (2015) Filled elastomers: a theory of filler reinforcement based on hydrodynamic and interphasial effects. J Mech Phys Solids 80:37–67. https://doi.org/10.1016/j.jmps.2015.04.012
28. Payne AR (1962) The dynamic properties of carbon black-loaded natural rubber vulcanizates. Part I J Appl Polym Sci 6:57–63. https://doi.org/10.1002/app.1962.070061906
29. Stoček R, Stěnička M, Maloch J (2020) Determining parametrical functions defining the deformations of a plane strain tensile rubber sample. In: Heinrich G, Kipscholl R, Stoček R (eds) Fatigue crack growth in rubber materials advances in polymer science, vol 286. Springer, Berlin, pp 19–38
30. Stoček R, Heinrich G, Gehde M, Kipscholl R (2013) Analysis of dynamic crack propagation in elastomers by simultaneous tensile and pure-shear mode testing. In: Heinrich G, Kaliske M, Klüppel M, Schneider K (eds) Fracture mechanics and statistical mechanics of reinforced elastomeric blends lecture notes in applied and computational mechanics, vol 70. Springer, Berlin, pp 269–301
31. Robertson CG, Stoček R, Mars WV (2020) The fatigue threshold of rubber and its characterization using the cutting method. In: Heinrich G, Kipscholl R, Stoček R (eds) Fatigue crack growth in rubber materials advances in polymer science, vol 286. Springer, Berlin, pp 57–83
32. Oskouyi AB, Uttandaraman Sundararaj U, Mertiny P (2014) Tunneling conductivity and piezoresistivity of composites containing randomly dispersed conductive nano-platelets. Mater 7:2501–2521. https://doi.org/10.3390/ma7042501
33. Efros AL, Shklovskii BI (1976) Critical behaviour of conductivity and dielectric constant near the metal-non-metal transition threshold. Phys Status Solidi B 76:475–485. https://doi.org/10.1002/pssb.2220760205
34. Bacon GE (1956) A method for determining the degree of orientation of graphite. J Appl Chem 6:477–481. https://doi.org/10.1002/jctb.5010061101
35. Pantea D, Darmstadt H, Kaliaguine S, Sümmchen L, Roy C (2001) Electrical conductivity of thermal carbon blacks: Influence of surface chemistry. Carbon 39:1147–1158. https://doi.org/10.1016/S0008-6223(00)00239-6
36. Noda T, Kato H, Takasu T, Okura A, Inagaki M (1966) The electrical resistivity of carbon black under compression. BCSJ 39:829–833. https://doi.org/10.1246/bcsj.39.829
37. Pantea D, Darmstadt H, Kaliaguine S, Roy C (2003) Electrical conductivity of conductive carbon blacks: influence of surface chemistry and topology. Appl Surf Sci 217:181–193. https://doi.org/10.1016/S0169-4332(03)00550-6
38. Jurkiewicz K, Pawlyta M, Burian A (2018) Structure of carbon materials explored by local transmission electron microscopy and global powder diffraction probes. C 4:68. https://doi.org/10.3390/c4040068

39. Shahamatifard F, Rodrigue D, Park KW, Frikha S, Mighri F (2021) Natural rubber nanocomposites: effect of carbon black/multi-walled carbon nanotubes hybrid fillers on the mechanical properties and thermal conductivity. Polym-Plast Technol Mater 60:1686–1696. https://doi.org/10.1080/25740881.2021.1930044